Cell

Planar Cell Polarity Links Axes of Spatial Dynamics in Neural-Tube Closure

Tamako Nishimura,[1,3] Hisao Honda,[1,2] and Masatoshi Takeichi[1,*]
[1]RIKEN Center for Developmental Biology, 2-2-3 Minatojima-Minamimachi, Chuo-ku, Kobe 650-0047, Japan
[2]Hyogo University, Kakogawa, Hyogo 675-0195, Japan
[3]Present address: Organization of Advanced Science and Technology, Kobe University, Nada-ku, Kobe 657-8501, Japan
*Correspondence: takeichi@cdb.riken.jp
DOI 10.1016/j.cell.2012.04.021

SUMMARY

Neural-tube closure is a critical step of embryogenesis, and its failure causes serious birth defects. Coordination of two morphogenetic processes—convergent extension and neural-plate apical constriction—ensures the complete closure of the neural tube. We now provide evidence that planar cell polarity (PCP) signaling directly links these two processes. In the bending neural plates, we find that a PCP-regulating cadherin, Celsr1, is concentrated in adherens junctions (AJs) oriented toward the mediolateral axes of the plates. At these AJs, Celsr1 cooperates with Dishevelled, DAAM1, and the PDZ-RhoGEF to upregulate Rho kinase, causing their actomyosin-dependent contraction in a planar-polarized manner. This planar-polarized contraction promotes simultaneous apical constriction and midline convergence of neuroepithelial cells. Together our findings demonstrate that PCP signals confer anisotropic contractility on the AJs, producing cellular forces that promote the polarized bending of the neural plate.

INTRODUCTION

Neural-tube closure is a key process for morphogenesis of the central nervous system. Failure in closure causes serious birth defects such as spina bifida and anencephaly, collectively called neural-tube defects. A number of genes are involved in neural-tube defects (Copp et al., 2003), but the causes of the defects are not fully understood. Neurulation proceeds sequentially with formation of the neural plate, bending of the plate, and closure of the bending plate to form a tube. At the cellular and molecular levels, it is thought that these processes are regulated by multiple mechanisms, including cellular intercalation, convergent extension of the neural plate, planar cell polarity (PCP) signaling, and actomyosin-dependent contraction of neuroepithelial layers. However, these mechanisms have never been integrated into a coherent story to explain neural-tube morphogenesis.

The intercalation of neuroepithelial cells is thought to produce a force required for the shaping of the neural plate. Cells in the plate move toward the midline, leading to their intercalation and the resultant convergent extension of this tissue (Keller et al., 1992). PCP signals (Simons and Mlodzik, 2008; Vladar et al., 2009) are required for the convergent extension (Wallingford et al., 2000; Ybot-Gonzalez et al., 2007); animals deficient in these signals fail to form a neural tube (Wallingford, 2006). How this PCP signal-dependent convergent extension is linked to closure of the plate is, however, poorly understood.

Bending of the neural plate involves the formation of both medial and dorsolateral hinge points. The median hinge point (MHP) occurs along the midline of the neural plate where neuroepithelial cells exhibit a wedge-like shape due to their apical constriction. This morphology of cells suggests that the MHP produces intrinsic forces to form the furrow on the neural plate (Schoenwolf, 1991). Extrinsic forces, produced by tissues located outside the neural plate, are also important in promoting the bending and folding of the neural plate (Alvarez and Schoenwolf, 1992). Genetic and cell biological analyses suggest that the bending of the neural plate and the apical constriction of neuroepithelial cells depend on Rho kinase (ROCK). Neuroepithelial cells adhere to each other via cadherin-based adherens junctions (AJs), which are located at the apical side of the neuroepithelial layer (Hong and Brewster, 2006). A scaffold protein, Shroom3, localized around the AJs, recruits ROCKs to the AJs (Hildebrand, 2005; Nishimura and Takeichi, 2008). ROCKs phosphorylate the regulatory light chains of myosin II, which is associated with the circumferential actin cables lining the AJs, leading to contraction of these actomyosin cables. Loss of Shroom3 impairs the closure of the neural plate (Haigo et al., 2003; Hildebrand and Soriano, 1999). Our current understanding of the role of ROCKs in neural-plate bending is, however, not sufficient to explain the overall mechanism. Neural-plate bending is polarized. It occurs only along the anterior-posterior axis of the embryo. This suggests that the cellular contractile system required for the bending is also polarized; otherwise the plate would bend only radially (Jacobson and Gordon, 1976). In support of this notion, the phosphorylated myosin light chain (pMLC) was detected only from a subset of AJs in the bending neural plate in chicken embryos (Nishimura and Takeichi, 2008). The mechanism to regulate this biased phosphorylation, however, remains to be determined.

The present study was designed to elucidate how AJ-associated actomyosin is activated in a polarized fashion in the

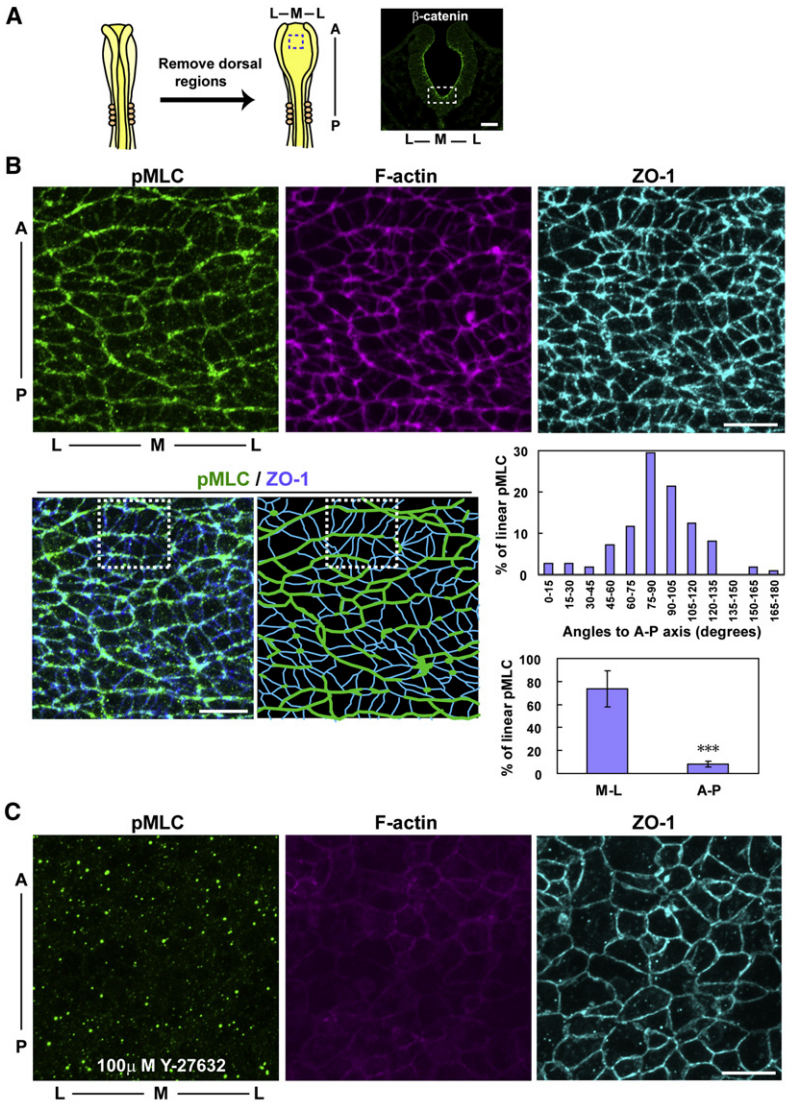

Figure 1. Mediolateral Orientation of Apical Actomyosin Cables at the Floor Plate

(A) Preparation of flat-mount specimen to observe the apical surface of the neural tube. Floor-plate regions of the midbrain area (marked with dotted squares) in stage 8 chicken embryos were selected for observation throughout the present analyses. A cross-section of a neural tube immunostained for β-catenin, an AJ protein, shows the area examined. M, midline; L, lateral side; A, anterior; P, posterior.

(B) The neural plate was stained for pMLC, F-actin, and ZO-1 in a flat-mounted stage 8 embryo and photographed from the apical side. The anterior side of neural plate is oriented toward the top, and the MHP is located along the vertical center of the photographs (this orientation of images is used in all figures). The merged image of stained pMLC and ZO-1 was traced. A portion showing their typical distributions is boxed (bottom). The top histogram shows the angular distribution of stained pMLC, quantified as follows: pMLC cables that linearly extended more than 10 μm across multiple cells in a 50 μm square region (20 to 30 cables per specimen) were selected, and the angles of the cables were measured relative to the A-P axis. The histogram shows the angular distribution determined from four specimens. The lower histogram shows the percent of the mediolateral (M-L, those angled from 60 to 120 degrees to the A-P axis) and anteroposterior (A-P, those angled from 0 to 30 degrees and from 150 to 180 degrees to the A-P axis) lines of pMLC. Data are the average of four specimens. Error bars, SD. ***$p < 0.001$ against the M-L-oriented pMLC.

(C) An embryo was treated for 3 hr with Y-27632 (100 μM), and its neural tube was prepared and stained as described in (B). Measurement of the apical surface area, outlined by ZO-1 staining, of individual cells in Y-27632-treated and -untreated embryos showed that the surface area increased 2.51 times ($n = 3$, $p < 0.05$) after the treatments. Scale bar, 10 μm.

See also Figure S1.

neural plate and how neuroepithelial cells respond to this local actomyosin activation in order to bend the plate. Our observations show that a set of PCP regulators function to locally activate ROCKs at the restricted set of AJs that are oriented toward the mediolateral axis of the neural plate, and that the resultant anisotropic contraction of the AJs causes the intercalation-like cell rearrangement as well as the mediolateral constriction of the plate. These sequential events result in induction of planar-polarized neural-plate bending.

RESULTS

Mediolateral Orientation of Active Actomyosin Cables Lining the AJ

The neural plate bends most drastically at the MHP. Based on the assumption that the bending along the midline of the neural plate is important for its entire closure, we focused on the MHP at the midbrain regions of chicken embryos. To observe the behavior of cells at the MHP, we opened the neural tubes of stage 8 embryos (Figure 1A) and immunostained whole-mount samples for several proteins localized in the AJs, which are located near the apical edge of neuroepithelial cell-cell contacts (Figure 1B). Staining for ZO-1 was used to delineate the apical borders of neuroepithelial cells. Contrasted with typical epithelial cells, which show a honeycomb-like arrangement, neural-plate cells display peculiar shapes at their apical plane and have both shorter and longer borders (Figure 1B). The shorter borders of each cell tended to link together linearly across multiple cells. F-actin colocalized with ZO-1 and was most highly condensed at the sites where the shorter borders clustered (Figure 1B).

The phosphorylated myosin light chain (pMLC, myosin light chain monophosphorylated at Ser19) is an activated form of myosin II. Staining of pMLC was highly enriched at the shorter borders (Figure 1B) and extended across multiple cells, resulting in a cable-like configuration. Individual cells displayed pMLC-rich and pMLC-poor borders in various patterns (Figure S1A available online). Some of these cells showed a bipolar distribution of pMLC; in these cells, the pMLC-rich borders were generally shorter than the pMLC-poor borders (Figure S1A), resulting

in a rectangular shape of the cells. Cells with this morphology were arranged in a ladder-like pattern, in which the pMLC-poor zones corresponded to the "steps" of the ladder (see the boxed region in Figure 1B for examples). In some cases, two ladders were aligned next to each other, sharing a single pMLC cable. Statistical analysis of the distribution of the pMLC cables showed that they tended to orient in a mediolateral direction (Figure 1B, bar graphs). In addition, punctate signals of pMLC were detected at the center of cell clusters with rosette-like configurations. Similar pMLC distributions were observed at the lateral sides of the neural plate (Nishimura and Takeichi, 2008). Vinculin, known to be an AJ-associated protein, was also distributed in a pattern similar to that of F-actin (see below), confirming that the cell junctions observed corresponded to AJs.

These observations suggested that the AJ-associated actomyosin was activated in a polarized fashion, inducing the anisotropic contraction of AJs. Treatment of embryos with Y-27632, an inhibitor of ROCKs, completely abolished the AJ-associated staining for pMLC (Figure 1C) and simultaneously inhibited neural-tube closure, as observed previously (Kinoshita et al., 2008; Wei et al., 2001; Ybot-Gonzalez et al., 2007). Furthermore, staining for AJ-associated F-actin became fainter, and cells lost polarity in their apical shapes and showed an increased apical area (Figure 1C), indicating that the contractility of AJs was entirely lost after Y-27632 treatments. These observations confirm that ROCK-dependent AJ contraction is essential for neural-tube closure.

We also examined embryos at different developmental stages. Mediolateral polarization of pMLC distribution was not observed in stage 5 embryos in which the neural plate was still flat. It became detectable after stage 6, when neural-plate bending begins (Figure S1B). In addition, we found that ppMLC (myosin light chain diphosphorylated at Thr18/Ser19), an indicator of more strongly and stably activated myosin II (Watanabe et al., 2007), was also distributed mediolaterally and colocalized with pMLC (Figure S1C), confirming the polarized activation of myosin II.

Live Imaging of Neural-Plate Cell Behavior

In order to investigate the cell behavior resulting from the polarized pMLC localization, we observed neural-plate cells by live imaging. We introduced plasmids encoding enhanced green fluorescent protein (EGFP)-tagged myosin light chain (MLC-EGFP) into stage 3 embryos by electroporation, so as to label AJs of the future neural plate. We confirmed that the exogenous expression of MLC-EGFP or EGFP alone in the neural plates had no effect on their bending or closure (Figures S2A and S2B). These control experiments also demonstrated that, in our electroporation protocol, expression of exogenous molecules tended to occur in the ventral sides of the neural plate, also in a mosaic fashion.

When embryos reached stage 7, we collected time-lapse images of labeled cells located along the midline, and we observed that the labeled cell masses underwent convergent extension (Figure 2A, top and Movie S1). Observations of individual cells revealed that there were two populations of MLC-labeled AJs, one contracted and the other extended during the 80 min observation period. There was a clear tendency for contraction to occur in mediolateral directions (Figure 2A, top, red lines and Figure S2C). In contrast, extension took place in anteroposterior directions (Figure 2A, top, blue lines). In addition, AJ contraction sometimes resulted in a rosette-like rearrangement of cells (Figure 2A, dotted circles), as seen during the germband elongation of *Drosophila* embryos (Blankenship et al., 2006). The rosettes were a transient structure: when these rosettes resolved, AJs re-extended in anteroposterior directions, although they remained contracted along the mediolateral axis. We also could observe the process of rectangular cell formation due to the constriction of the two opposing edges of a cell (Figure 2A, arrowheads).

When embryos were treated with Y-27632, no such contraction or extension of AJs occurred. Labeled cells stayed at constant positions during the observation (Figure 2A, bottom and Movie S2). This suggests that the polarized shrinking and extension of AJs were responsive for the intercalation-like rearrangement of cells. During these observations, we did not detect any free movement of cells toward the midline, indicating that these cellular rearrangements appeared to be solely dependent on the apical junctional remodeling.

Mathematical Modeling of Supracellular Actomyosin Cable Formation

We wondered how the AJ-associated actomyosin organized into the linear supracellular cables. We suspected that the mediolateral contraction of AJs might be responsible for this patterning. To verify this idea, we made use of mathematical modeling. One of us previously proposed the "dynamic cell model" to explain epithelial cell patterning (Honda et al., 2008; Nagai and Honda, 2001). In this model, a polygonal pattern, where polygons are packed in a two-dimensional space, imitates the epithelial sheets. We introduced anisotropic contraction of the edges into the dynamic cell model. Figure 2B (step 0) shows a polygonal pattern with uniform contraction of its edges. We then applied additional contractile forces, only to the edges inclined 0 to 15 degrees from the horizontal axis, and collected snapshots of the changing patterns at varying steps (0 to 180). By step 120, a certain group of polygons organized into horizontal arrays, where several edges linked with each other to form a straight chain, with a direction biased toward the horizontal axis. At step 180, polygons composing these arrays shortened along the horizontal axis, whereas they expanded along the vertical axis, assuming a ladder-like arrangement. By analyzing detailed changes of a particular group of polygons, we noted that the polygon pattern changes involve their intercalation as well as rosette-like rearrangement (Figure 2B, squared area). The resultant overall pattern of the polygons is similar to the cellular pattern observed at the apical plane of the neural plate. These results support the idea that the contraction of individual AJs along mediolateral directions autonomously reorganizes them into supracellular lines.

Celsr1 Determines the Mediolateral Polarity of Actomyosin Activation

Next, we asked which mechanism determines the mediolateral activation of actomyosin. The pattern of pMLC staining seen in the neural plate (Figure 1B) suggested that PCP signaling may

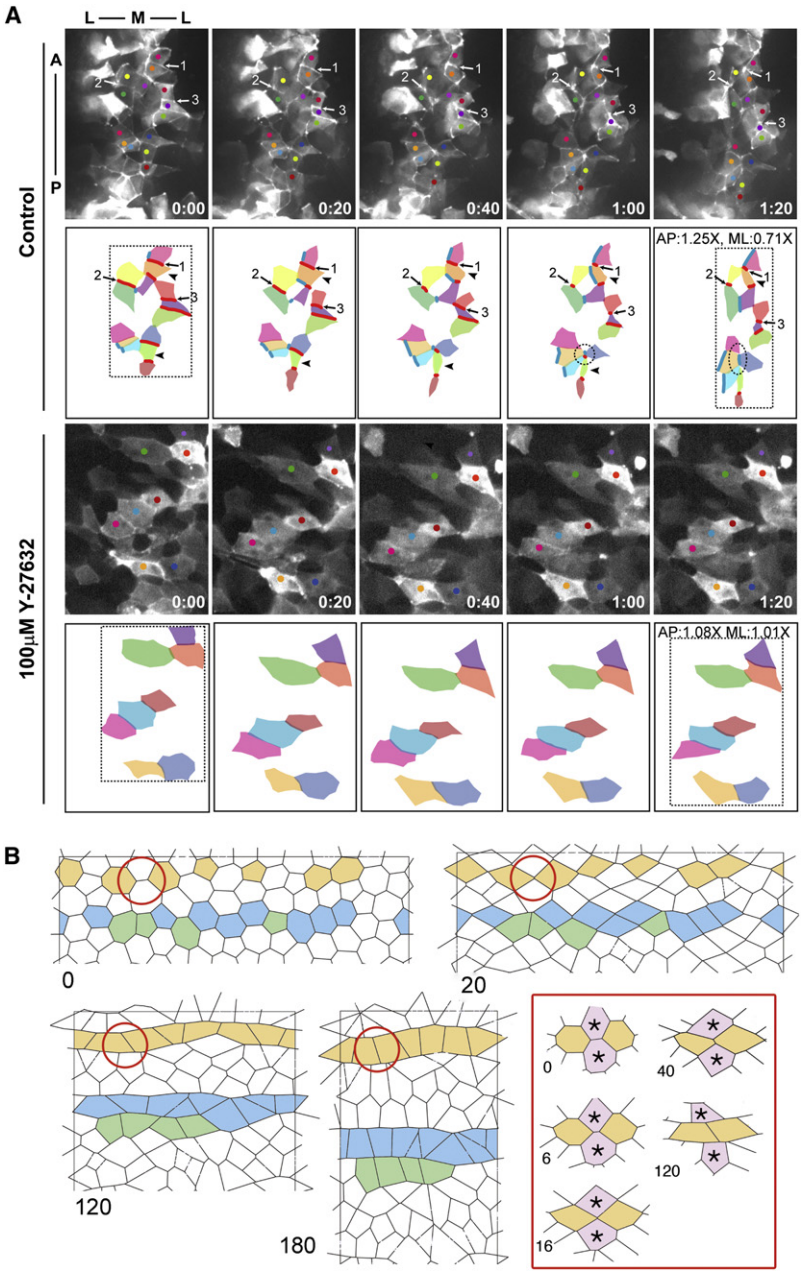

Figure 2. Analyses of Neuroepithelial Cell Rearrangement

(A) Time-lapse imaging of neuroepithelial cells transiently transfected with plasmids encoding MLC-EGFP. Photos at 20 min intervals are shown. Top, control embryo; bottom, embryo treated with Y-27632 as described in the legend of Figure 1C. The anterior side is at the top, and the MHP is at the vertical center. Schematic diagrams delineating the apical junctions are shown below each picture. Examples of shrinking and extending junctions are shown in red and blue, respectively. The area occupied by the cells depicted here is shown with a square. During the observation period of the control embryo, the area's anterior-posterior (A-P) edge increased 25%, and the mediolateral (M-L) edge decreased 29%. Minimal changes were observed in Y-27632-treated embryos. Circles indicate examples of rosettes, which formed at time 0:50 and resolved afterwards. Arrowheads show cells that transformed their shape into a rectangular one. A typical example of six independent experiments is shown for each sample.

(B) Mathematical modeling of cell junctional rearrangement. Polygonal cellular patterns are shown under uniform (step 0) and anisotropic (steps 20 to180) contraction of the edges. In the square, detailed changes of four polygons, marked with red circles, are shown. Two polygons labeled with asterisks initially contact one another with a horizontal edge, but this edge shortens at steps 6 and 16. This edge is then replaced with a new contact formed between the other pair of polygons, and this expands vertically at steps 40 and 120. See the Extended Experimental Procedures for details.

See also Figure S2 and Movies S1 and S2.

be involved. Immunohistochemical analysis for Celsr1, a vertebrate homolog of *Drosophila* Flamingo (one of the core PCP members), showed that it is localized at the apical side of the neural tube (Figure 3A, left). This protein is known to be required for neural-tube closure and other PCP-related events (Curtin et al., 2003; Devenport and Fuchs, 2008; Ravni et al., 2009). Celsr1 colocalized with the condensed F-actin (Figure 3A, right) or pMLC (Figure S3A). Celsr1 was typically located at the shorter edges of cells (see the boxed area in Figure 3A as an example). This polarized distribution of Celsr1 was not seen at stage 5 but began at stage 6 and correlated with the onset of the polarized arrangement of pMLC (Figure S3B). Previous in situ hybridization experiments showed that, although the neural plate expresses Celsr1 transcripts, early floor-plate cells do not (Formstone and Mason, 2005). It is therefore possible that we are observing the apical edges of peri-floor-plate cells but not of floor-plate cells, which probably intermingle at the midline region.

To determine the role of Celsr1, we depleted it by electroporating Celsr1-specific small interfering RNAs (siRNAs) into neural plates. Celsr1 knockdown (KD) caused neural-tube closure defects (Figure 3B). Similar results were obtained using two independent Celsr1-specific siRNA oligos, but none of the control oligos showed such effects (Figure S3C). In Celsr1-depleted neural plates, the concave shape of their apical edges was lost at the ventral regions. It became flat, or even convex, and the ratio of the apical to basal edge widths increased significantly (Figure 3B, bottom bar graph). These KD effects were less visible at the dorsolateral areas of the neural plate; this is likely due to the biased incorporation of siRNAs in the ventral regions (see Figure S2A). At the lateral sides of these tubes, the neural plates tended to exhibit a sharper inner curvature than in control embryos. This excess bending was likely produced as a result of the connection between the unaffected dorsal portion and the flattened ventral portion of the plate.

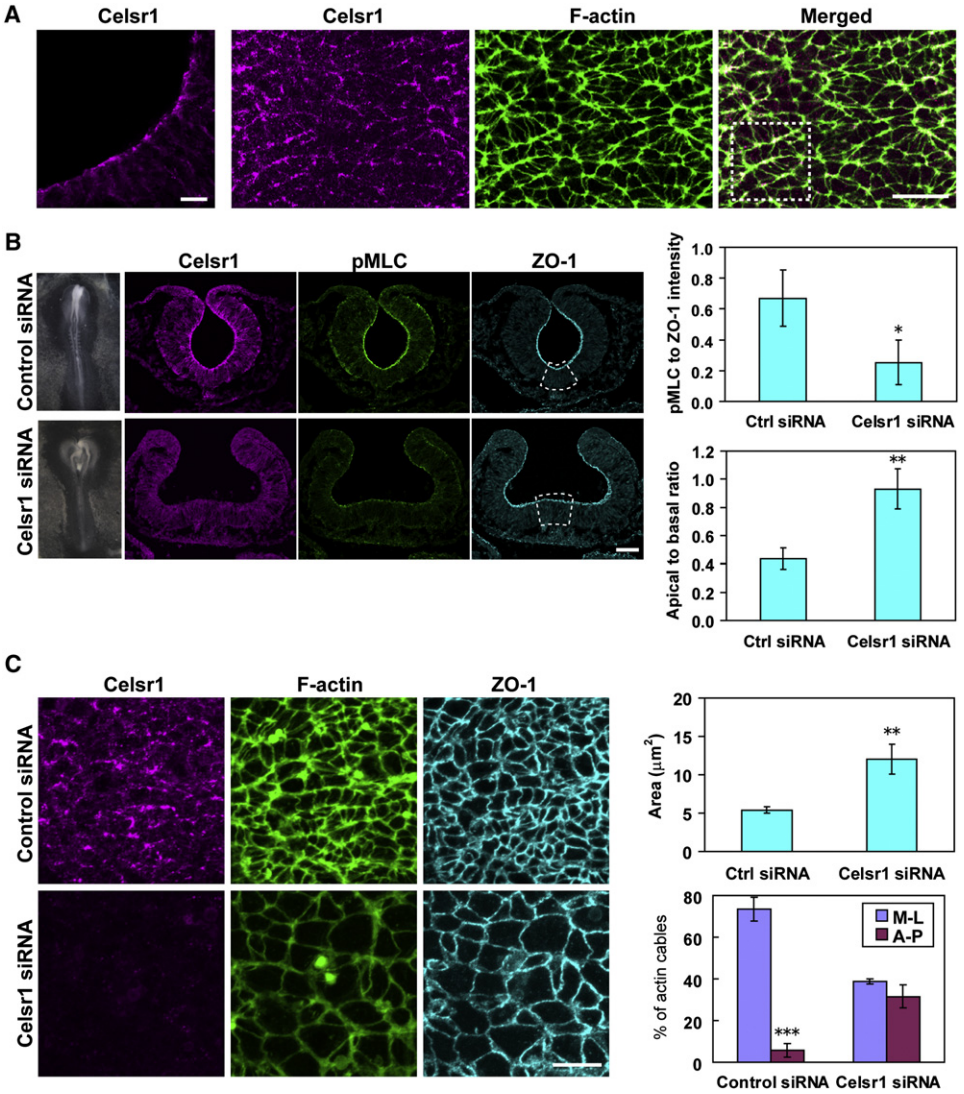

Figure 3. Celsr1 Is Required for the Mediolateral Distribution of Actomyosin Cables

(A) Left,ilmmunostaining for Celsr1 in a transverse section of the neural plate at stage 8. Scale bar, 50 μm. Right, costaining for Celsr1 and F-actin in a flat-mount of the neural plate at the same stage. Celsr1 colocalizes with condensed F-actin cables. A portion showing a typical pattern of Celsr1 and F-actin distributions is boxed. Scale bar, 10 μm.

(B) Effects of Celsr1 KD on neural-tube bending. Embryos were electroporated with Celsr1-specific or scrambled (control) siRNAs and fixed at stage 8. Left, whole embryos; right, transverse sections at a midbrain level costained for Celsr1, pMLC, and ZO-1. Scale bar, 50 μm. Histograms, the ratio of the immunofluorescence intensity of pMLC to ZO-1 (upper), and the ratio of the apical edge width to the basal edge width of the neural plate (lower). Data were collected from the enclosed areas of sectioned neural plates. Histograms represent an average of three specimens. Error bars, SD. *$p < 0.05$, **$p < 0.01$. Similar results were obtained with another independent siRNA oligo (Figure S3C).

(C) Effects of Celsr1 KD, performed as explained in (B), on the mediolateral condensation of actin cables. Left, costaining for Celsr1, F-actin, and ZO-1 at the apical surface of the neural tube in an embryo treated as in (B). Scale bar, 10 μm. Right, the apical surface area and the polarity of condensed actin cables were quantified. Areas of the apical surface, outlined by ZO-1, were measured in a 50 μm square region. In the same region, actin cables that linearly extend more than 10 μm across multiple cells were counted; those that cover only a single cell were not counted. Histograms represent an average of three specimens. Error bars, SD. **$p < 0.01$, ***$p < 0.001$.

See also Figure S3 and Movie S3.

In the neural plates electroporated with Celsr1 siRNAs, apical pMLC staining was reduced (Figure 3B, top bar graph). Analysis of the apical view of Celsr1-KD plates (Figure 3C) showed that the polarized condensation of F-actin was abolished, and the apical surface area of individual cells was enlarged (Figure 3C). The polarized localization of pMLC was also abolished, although residual pMLC signals remained along AJs (Figure S3A). Live imaging of EGFP-MLC in Celsr1-KD neural plates showed that their convergence-extension was suppressed (Movie S3). The edges of individual cells still exhibited contraction or extension

to some extent but without particular polarities (Figure S2D). These results suggest that, in the absence of Celsr1, residual pMLC is still functional but cannot confer the directional contractility on cellular edges.

As Celsr1 is expected to cooperate with other core members of PCP, we chose to analyze one of them, Dishevelled, for its potential involvement in the polarized actomyosin activation. Dishevelled deficiencies are known to cause neural-tube defects (Etheridge et al., 2008; Hamblet et al., 2002; Wang et al., 2006). We found that Dishevelled-2, one of multiple isoforms, is localized at the apical portion of the neural tube in chicken embryos, exhibiting a mediolateral linear orientation (Figure S3D). To block the functions of Dishevelled, we used a dominant-negative Dishevelled, Xdd1 (Sokol, 1996). When Xdd1 was expressed in the neural plates, the treated embryos showed phenotypes similar to those found after Celsr1 depletion (Figure S3E). These results suggest that Celsr1 may cooperate with Dishevelled. Cell biology studies confirmed their cooperation (see below).

PDZ-RhoGEF Regulates Polarized Actomyosin Activation

There are likely to be mediators that link the Celsr1/Dishevelled-dependent PCP signaling and ROCK-dependent myosin II activation. Dishevelled is known to regulate Rho (Habas et al., 2001; Strutt et al., 1997; Winter et al., 2001). To identify such mediators, we screened Rho guanine nucleotide exchange factors (RhoGEFs), which can activate ROCKs via RhoA activation. Among several candidates, we found that *PDZ-RhoGEF* (*ARHGEF11*) transcripts were highly expressed in the neural tube, and PDZ-RhoGEF proteins were localized at the apical side of neural plates (Figure 4A, left). PDZ-RhoGEF is one of the vertebrate homologs of *Drosophila* RhoGEF2, which is known to regulate mesoderm invagination during gastrulation (Häcker and Perrimon, 1998; Kölsch et al., 2007). In the apical surface of chicken embryonic neural plates, PDZ-RhoGEF was concentrated along the pMLC cables (Figure 4A, right).

siRNA-mediated depletion of PDZ-RhoGEF prohibited neural-tube closure (Figure 4B). Similar results were obtained using two independent PDZ-RhoGEF-specific siRNA oligos (Figure S4A). PDZ-RhoGEF depletion caused the loss of the polarized contraction of F-actin, as well as the enlargement of the apical surface area of cells (Figure 4C), as seen in the case of Celsr1 KD. Staining of pMLC was also reduced, and its polarized condensation was abolished (Figures 4B and S4B). Live imaging of PDZ-RhoGEF KD neuroepithelial cells indicated that the convergent-extension of neural plates was blocked, but the contractility of cellular edges was still detectable (Movie S4 and Figure S2D), as seen in Celsr1 KD embryos: this possibly depended on residual pMLC. In addition, PDZ-RhoGEF colocalized with vinculin, providing further evidence for its association with AJs (Figure S4C): PDZ-RhoGEF depletion perturbed the junction morphologies that are outlined with vinculin, as expected. In sum, these results suggest that PDZ-RhoGEF is involved in the polarized actomyosin contraction in the neural plate.

DAAM1 Interacts with PDZ-RhoGEF

We next sought mechanisms that link the functions of Celsr1/Dishevelled and PDZ-RhoGEF. DAAM1, one of the formins that play a role in F-actin polymerization (Lu et al., 2007), is known to interact with Dishevelled at its C-terminal region and with active RhoA at its N-terminal region (Habas et al., 2001). DAAM1 is autoinhibited via the interaction between its N- and C-terminal domains, and this process is blocked through binding to Dishevelled (Liu et al., 2008). Immunohistochemical staining showed that DAAM1 is distributed at the apical portion of the neural plate (Figure 5A) and colocalized at cell-cell borders with ZO-1, without exhibiting distinct polarities (Figure 5B, and also see Figure S6A). DAAM1 depletion again inhibited neural-tube closure (data not shown). Importantly, DAAM1 interacted with PDZ-RhoGEF. To demonstrate this interaction, we prepared 293T cells cotransfected with plasmids that expressed Myc-tagged DAAM1 and FLAG-tagged PDZ-RhoGEF. The two molecules could be coprecipitated from the lysates of these cells (Figure 5C). Endogenous DAAM1 could also be coprecipitated with FLAG-tagged PDZ-RhoGEF (Figure 5D). When we used a set of deletion mutants of DAAM1 and PDZ-RhoGEF, tagged with Myc and FLAG, respectively, the C-terminal half of DAAM1 containing FH1 and FH2 regions (DAAM1-C) interacted with the C-terminal half of PDZ-RhoGEF containing DH and PH regions (PDZR-DHPH) (Figure S5). These results indicate that DAAM1 and PDZ-RhoGEF can form a complex.

Previous reports showed that mDia, another formin, interacts with LARG, and that this interaction enhances the GEF activity of LARG (Kitzing et al., 2007). Therefore, we examined whether the interaction of DAAM1 and PDZ-RhoGEF similarly enhances the GEF activity of PDZ-RhoGEF. First we analyzed the interaction between DAAM1-C and GST-tagged PDZR-DHPH proteins. A GST-pulldown assay confirmed that their interaction occurred (Figure 5E, left). Next, we measured the RhoGEF activity of PDZR-DHPH in the presence or absence of DAAM1-C. The presence of a 2.5-fold or 5-fold excess of DAAM1-C protein increased the activity of PDZR-DHPH in a dose-dependent manner (Figure 5E, right). These results support the idea that DAAM1 can enhance the GEF activity of PDZ-RhoGEF.

Interaction between DAAM1 and PDZ-RhoGEF Depends on Dishevelled

We next asked whether the interaction between DAAM1 and PDZ-RhoGEF is regulated by Dishevelled. First, we looked at the interaction between DAAM1 and PDZ-RhoGEF in the presence or absence of a dominant-negative Dishevelled, Xdd1. Immunoprecipitation studies using lysates from 293T cells transfected with appropriate expression plasmids demonstrated that the interaction of DAAM1 and PDZ-RhoGEF was greatly reduced in cells expressing Xdd1 (Figure 5F). We next examined the effect of depletion of endogenous Dishevelled on the interaction between DAAM1 and PDZ-RhoGEF. 293T cells express Dishevelled-2 and -3 but not Dishevelled-1 (data not shown). We therefore knocked down Dishevelled-2 or -3 or both in 293T cells transfected with plasmids expressing DAAM1 and PDZ-RhoGEF. The binding between DAAM1 and PDZ-RhoGEF decreased with depletion of either Dishevelled-2 or -3 and was almost undetectable after depletion of both (Figure 5G). These results support the idea that the interaction of DAAM1 and PDZ-RhoGEF occurs under the control of Dishevelled that can relieve DAAM1 from its autoinhibited state. In the experiments

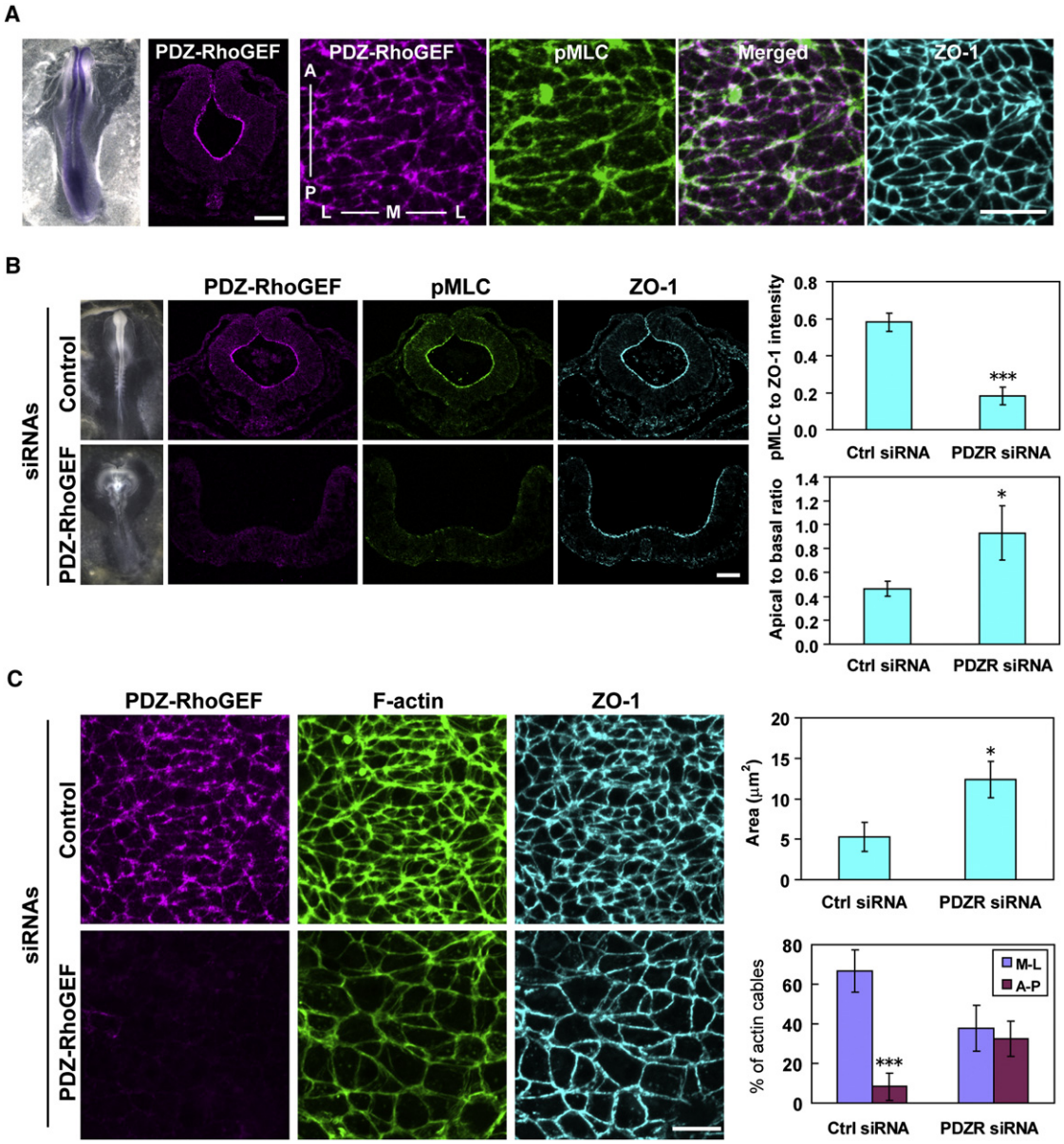

Figure 4. PDZ-RhoGEF Is Important for Mediolateral Contraction of Actomyosin

(A) Left, whole-mount in situ hybridization for *PDZ-RhoGEF* in a stage 8 embryo. Middle, immunostaining for PDZ-RhoGEF in a transverse section of a neural tube from a stage 8 embryo. Scale bar, 50 μm. Right, coimmunostaining for PDZ-RhoGEF, pMLC, and ZO-1 at the apical surface of the floor plate. Scale bar, 10 μm.
(B) PDZ-RhoGEF was depleted as described for Celsr1 KD (see Figure 3B legend). Left, whole embryos are shown; right, transverse sections costained for PDZ-RhoGEF, pMLC, and ZO-1. Scale bar, 50 μm. Histograms, the ratio of the immunofluorescence intensity of pMLC to ZO-1 (upper), and the ratio of the apical edge width to the basal edge width of the neural plate (lower). These data were collected as explained in the Figure 3B legend. Histograms represent an average of three specimens. PDZR, PDZR-RhoGEF. Error bars, SD. *$p < 0.05$, ***$p < 0.001$. Similar results were obtained with another independent siRNA oligo (Figure S4A).
(C) Effects of PDZ-RhoGEF KD on the distribution of actin cables. Left, costaining for PDZ-RhoGEF, F-actin, and ZO-1 at the apical surface of the neural tube in an embryo treated as in (B). Scale bar, 10 μm. Right, quantitative analysis of the apical surface area and the polarity of actin cables. See Figure 3C legend for methods. Histograms represent an average of three specimens. Bars, SD. *$p < 0.05$, ***$p < 0.001$.
See also Figure S4 and Movie S4.

shown in Figure 5E, DAAM1-C could bind to PDZ-RhoGEF in a Dishevelled-free condition. DAAM1-C is probably not autoinhibited because this mutant lacks the N-terminal regions required for intramolecular interactions, and it may not require Dishevelled for the binding to PDZ-RhoGEF.

PCP Pathway Members Recruit PDZ-RhoGEF to Cell Junctions

To confirm the signaling pathway from Celsr1 to actomyosin contraction, we conducted cell biology studies. To examine how Celsr1 and Dishevelled cooperate, we prepared MDCK

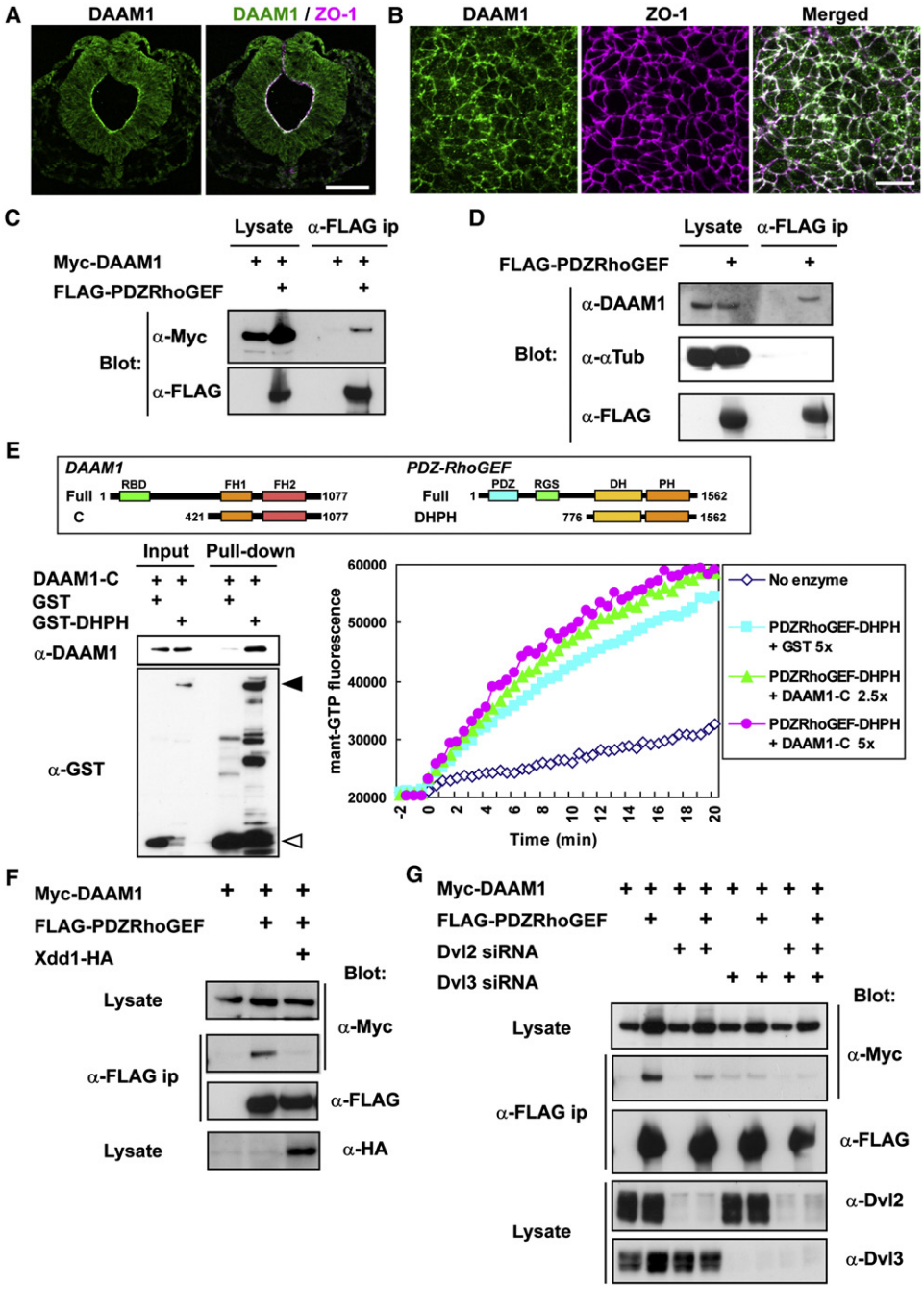

Figure 5. DAAM1 Interacts with PDZ-RhoGEF in the Presence of Dishevelled

(A) Coimmunostaining for DAAM1 and ZO-1 in a transverse section of a stage 8 neural tube. Scale bar, 50 μm.

(B) Coimmunostaining for DAAM1 and ZO-1 at the apical surface of the floor plate. Scale bar, 10 μm.

(C) Interaction of DAAM1 with PDZ-RhoGEF. 293T cells were cotransfected with plasmids expressing Myc-tagged DAAM1 and FLAG-tagged PDZ-RhoGEF or Myc-tagged DAAM1 alone, as indicated by "+" above the immunoblots. Cell lysates were subjected to immunoprecipitation with anti-FLAG antibody, followed by immunoblotting with antibodies against Myc or FLAG, as indicated.

(D) Interaction of endogenous DAAM1 with PDZ-RhoGEF. 293T cells were transfected with FLAG-tagged PDZ-RhoGEF or an empty vector. Cell lysates were subjected to immunoprecipitation with anti-FLAG antibody, followed by immunoblotting with antibodies against DAAM1, α-tubulin (αTub), or FLAG, as indicated.

(E) Effects of DAAM1 on the RhoGEF activity of PDZ-RhoGEF. Top, schematic representation of the deletion mutants of DAAM1 and PDZ-RhoGEF. Bottom-left, in vitro binding of DAAM1-C with PDZ-RhoGEF-DHPH. Purified DAAM1-C, GST, or GST-DHPH were mixed as indicated by the "+" above the immunoblots. Proteins were pulled down with GSH-Sepharose, followed by immunoblotting with anti-DAAM1 or anti-GST antibodies, as indicated. Closed arrowhead, GST-PDZ-RhoGEF-DHPH; open arrowhead, GST. Bottom-right, RhoGEF activity of PDZ-RhoGEF in the presence or absence of DAAM1. PDZ-RhoGEF-DHPH was incubated with a 2.5- or 5-fold excess of DAAM1-C (closed triangles and closed circles, respectively) or a 5-fold excess of GST (closed squares). A mixture

cells transiently expressing each molecule. When Celsr1-expressing cells were in contact with each other, Celsr1 was concentrated at cell-cell contacts (Figure 6A, left), as predicted from Celsr1's homophilic binding nature (Usui et al., 1999). In contrast, when Dishevelled-2 was expressed in MDCK cells, this molecule was diffusely distributed in the cytoplasm. However, when Celsr1 and Dishevelled-2 were coexpressed, Dishevelled-2 became sharply associated with the Celsr1-positive contact sites (Figure 6A, right top). Because Frizzled is known to recruit Dishevelled to the cell membrane, we also looked at the behavior of HA-tagged Frizzled-6. Frizzled-6 expressed alone in MDCK cells was distributed in the cytoplasm (data not shown). However, when Dishevelled-2, Frizzled-6, and Celsr1 were expressed in the same cell, both Dishevelled-2 and Frizzled-6 were found at Celsr1-positive cell-cell junctions (Figure 6A, right bottom). These findings suggest that the three proteins organize into a complex, consistent with the general view of their interaction (Vladar et al., 2009).

We next analyzed the relations between DAAM1, Celsr1, and Dishevelled. We prepared MDCK cells stably expressing DAAM1 (MDCK-DAAM1). In these cells, DAAM1 was ubiquitously localized along the AJs, colocalizing with αE-catenin and F-actin (Figure 6B). When Dishevelled-2 was expressed in the MDCK-DAAM1 cells, Dishevelled-2 remained in the cytoplasm (Figure 6C, top), suggesting that the interactions between these two molecules require other mediators. When Dishevelled-2 was coexpressed with Celsr1, however, Dishevelled-2 was found at the Celsr1-positive cell-cell junctions, as described above, resulting in its colocalization with DAAM1 (Figure 6C, bottom).

We then examined whether these molecules regulate the localization of PDZ-RhoGEF. PDZ-RhoGEF, which was expressed in MDCK cells, distributed mainly in the cytoplasm, with only a small amount detected in the apical portion of cell junctions. The distribution was not changed in the presence of Dishevelled-2 and Celsr1 (Figure 6D, top). However, when PDZ-RhoGEF, Dishevelled-2, and Celsr1 were all coexpressed in MDCK-DAAM1 cells, PDZ-RhoGEF was more clearly detected at the junctions expressing both Dishevelled-2 and Celsr1, and its amount correlated with the amounts of the others (Figure 6D, bottom and right). These results indicate that PDZ-RhoGEF becomes associated with the Dishevelled-2- and Celsr1-localizing junctions through its interaction with DAAM1. These findings are consistent with our biochemical results (Figure 5).

Celsr1 Determines the Polarized Distribution of PDZ-RhoGEF and ROCK1

To confirm the in vivo linkage between Celsr1 and PDZ-RhoGEF or its downstream effector ROCK1, we compared their distribution in the neural plate. Celsr1 colocalized with condensed fractions of PDZ-RhoGEF and also with ROCK1 (Figures 7A and 7B). Quantitation of the distribution of these molecules as well as Dishevelled confirmed that all of them tended to localize in mediolateral directions (Figure S6A). When Celsr1 was knocked down, both PDZ-RhoGEF and ROCK1 became diffuse. Conversely, in PDZ-RhoGEF-depleted or Y-27632-treated neural plates, Celsr1 immunofluorescence signals were still detectable as distinct clusters on AJs, although the AJs were now expanded (Figures S6B). These Celsr1 clusters were located at only limited portions of the AJs, as revealed by costaining for Celsr1 and ZO-1, indicating that their distribution is still polarized. These observations confirmed that Celsr1 functions upstream of the PDZ-RhoGEF and ROCK1 condensing processes, and also that Celsr1 cannot regulate AJ contractility in the absence of PDG-RhoGEF.

We also conducted cell biology studies to further test whether ROCK1 recruitment to cell junctions is dependent on Celsr1 and distal molecules in its pathway. In MDCK and MDCK-DAAM1 cells, endogenous ROCK1 is only faintly condensed along the AJs. However, when Celsr1, Dishevelled-2, and PDZ-RhoGEF were condensed together in AJs of MDCK-DAAM1 cells, ROCK1 was upregulated at these specific junctions (Figure 6E). Unless the junctional accumulation of PDZ-RhoGEF was detectable, ROCK1 was not upregulated in the junctions of these model cells.

DISCUSSION

Our findings collectively suggest the following processes, which lead to neural-plate bending (Figure 7C): (1) Celsr1 distributes along a subpopulation of AJs that is oriented toward the mediolateral axis of the neural plate. (2) Dishevelled is recruited to the Celsr1-positive junctions together with Frizzled. (3) DAAM1 uniformly distributes at the AJs and is activated via the interaction with Dishevelled. (4) Activated DAAM1, in turn, activates PDZ-RhoGEF via their physical interactions. (5) PDZ-RhoGEF recruits ROCKs to these sites, probably by activation of RhoA. (6) ROCKs activate myosin II by phosphorylating MLC. (7) Actomyosin associated with these AJs contracts along the mediolateral axis, organizing into a cable across multiple cells. (8) At the cellular level, this contraction causes a convergent

containing a fluorogenic substrate (mant-GTP) was added at time 0, and the increase in the fluorescence intensity was measured. "No enzyme" (open diamonds) indicates a sample incubated with substrate alone. Each value represents an average of two reactions.

(F) Interaction of DAAM1 and PDZ-RhoGEF in the presence of dominant-negative Dishevelled (Xdd1). 293T cells were cotransfected with plasmids expressing Myc-tagged DAAM1 and FLAG-tagged PDZ-RhoGEF without or with a plasmid expressing HA-tagged Xdd1 as indicated by the "+" above the immunoblots. Cell lysates were subjected to immunoprecipitation with anti-FLAG antibody, followed by immunoblotting with antibodies against Myc, FLAG, or HA tags, as indicated.

(G) Interaction of DAAM1 and PDZ-RhoGEF in Dishevelled-2/3-depleted cells. 293T cells were cotransfected with plasmids expressing Myc-tagged DAAM1 and FLAG-tagged PDZ-RhoGEF together with siRNAs for Dishevelled-2 or -3 or both, as indicated by the "+" above the immunoblots, or with control siRNA (si2, not indicated). Cell lysates were subjected to immunoprecipitation with anti-FLAG antibody, followed by immunoblotting with antibodies against Myc, FLAG, or Dishevelled-2 or -3, as indicated.

See also Figure S5.

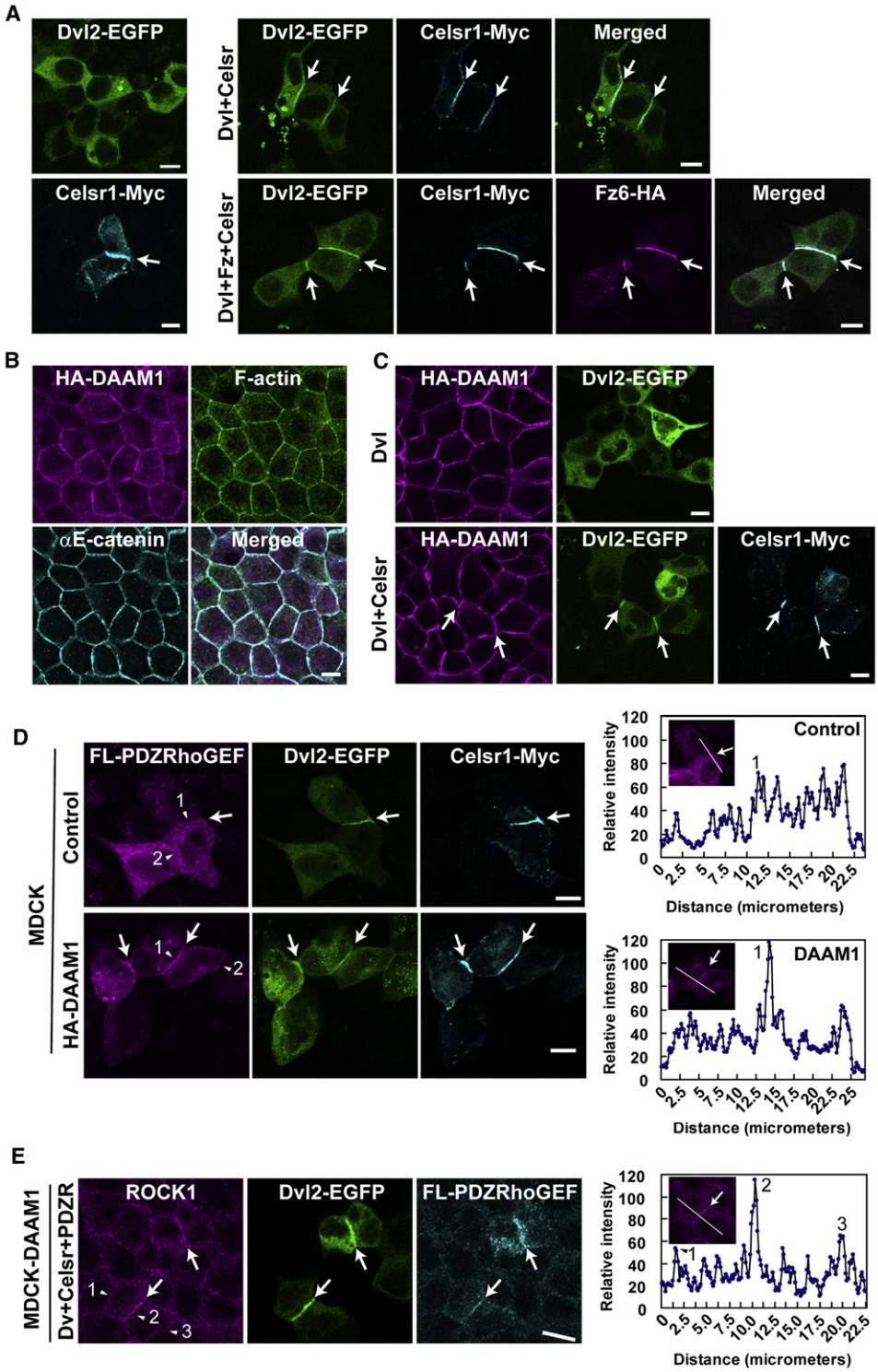

Figure 6. Celsr1-, Dishevelled-, and DAAM1-Dependent Recruitment of PDZ-RhoGEF and ROCK1 in MDCK Cells

(A) Colocalization of Dishevelled, Celsr1, and Frizzled-6 at MDCK cell junctions. Left, cells were transfected with a plasmid expressing EGFP-tagged Dishevelled-2 (Dvl2-EGFP) or one expressing Myc-tagged Celsr1 (Celsr1-Myc). Right, cells were cotransfected with plasmids expressing Dvl2-EGFP and Celsr1-Myc or triple-transfected with these constructs and HA-tagged Frizzled-6 (Fz6-HA). Arrows point to cell-cell contacts where these proteins accumulated. Scale bars, 10 μm.

(B) HA-tagged DAAM1 (HA-DAAM1), stably expressed in MDCK cells, was immunostained together for αE-catenin and F-actin. Scale bar, 10 μm.

relocation of cells toward the midline of the neural plate, resulting in a mediolateral shortening of the plate at its apical edge. These sequential events explain how neuroepithelial cells use PCP signals for the convergent extension, apical constriction, and eventual bending of their sheets.

How Is Celsr1 Localization Determined in the Neural Plate?

How Celsr1 is recruited to specific AJs remains unknown. In rectangular-shaped cells, Celsr1 localized at the shorter edges in a bipolar fashion. This feature of Celsr1 distribution is reminiscent of that of Flamingo, the *Drosophila* ortholog of Celsr1, in developing wings (Usui et al., 1999). It is thought that a graded expression of Fat-Dachsous signals along the distal-to-proximal axis of the wing primordium determines this pattern of Flamingo localization (McNeill, 2010). Similar or other upstream mechanisms might regulate Celsr1 localization in the vertebrate neural plate. It is of note that, during gastrulation in *Drosophila* embryos, future mesodermal cells undergo anisotropic cell-shape changes, which are, in part, similar to those occurring in neural-plate cells. It was proposed that the tissue tension generated by individual cells along the anteroposterior axis resulted in such cell-shape changes (Martin et al., 2010). Similar forces could signal Celsr1 to localize at particular sites of neuroepithelial AJs. However, even when AJ contractility was abolished with ROCK inhibitors, Celsr1 was still found clustered at localized sites. This suggests that mechanical forces alone may not be sufficient to determine Celsr1 localization.

Signaling from Celsr1 to Rho Kinase

Our observations suggested that Celsr1, Dishevelled, and Frizzled autonomously form a tripartite complex, consistent with the observations in *Drosophila* (Chen et al., 2008). Our in vitro studies indicated that Dishevelled has the ability to enhance the binding of DAAM1 to PDZ-RhoGEF, and that DAAM1 can activate PDZ-RhoGEF via binding. PDZ-RhoGEF was concentrated at junctions only when Celsr1, Dishevelled, and DAAM1 were accumulated together, and ROCK1 was recruited to these junctions. These observations suggest that the initial Celsr1-Celsr1 interactions create a platform to activate the RhoGEF-ROCK system at selected AJs. On the other hand, it is known that DAAM1 can directly control the actin cytoskeleton as a formin-family protein, and this protein is even required for normal AJ formation (Aspenström et al., 2006; Li et al., 2011). Therefore, DAAM1 may also regulate AJ formation through a Celsr-independent pathway (Figure 7C).

Neuroepithelial cells exhibited their peripheral motility even when Celsr1 was depleted, suggesting that the AJs have a Celsr1-independent contractility. This ability of AJs could depend on other ROCK regulators such as Shroom3. Shroom3 is a scaffold protein to recruit ROCKs to the AJs, and this function of Shroom3 is required for neural-tube morphogenesis (Hildebrand and Soriano, 1999; Nishimura and Takeichi, 2008). It is likely that the role of Celsr1 is to restrict junctional contractility to specific AJs, whereas Shroom3 plays a more basic role in AJ contraction.

How Does the Neural Plate Bend?

A classic model to explain neural-tube bending is that neural epithelial cells constrict at the apical side, and this constriction leads to inward bending of the neural plate. However, this model does not explain the polarized bending of the plate. We have now demonstrated that the contraction of cellular edges occurs in a PCP-dependent manner. The pattern of the AJ-associated actomyosin networks was complex; nevertheless, there was a clear tendency for the activated actomyosin cables to be oriented along the mediolateral axis. Our mathematical simulation corroborated the idea that the overall pattern of these cables reflects the mediolaterally biased contraction of individual AJs. Thus, our observations indicate that, at the tissue level, PCP-mediated contraction of individual AJs (located only at the apical side of the plate) produces a force that constricts the apical plane of the neural plate along the mediolateral axis. This constriction should occur only at the ''free'' apical plane of the plates because the basal surfaces of neuroepithelial cells are structurally fixed to the extracellular matrices. Under this three-dimensional condition, the mediolateral contractile forces, operating on the apical surface of the neural plate, are expected to cause its polarized, inward bending.

At the cellular level, anisotropic contractions of AJs caused an intercalation-like relocation of cells, including their transient rearrangement into rosette-like clusters. These cells never moved freely at least at the apical plane; thus, only the junctional remodeling appeared to drive these cellular rearrangements. As the axis and timing of the cellular contraction-extension fluctuated among the cells, the overall change of the neural-plate shape should be a result of the sum of the fluctuating behaviors of individual cells.

(C) HA-DAAM1-expressing MDCK cells were transfected with a plasmid expressing Dvl2-EGFP with or without a plasmid expressing Celsr1-Myc. Arrows point to cell-cell contacts where these proteins accumulated. Scale bar, 10 μm.

(D) FLAG-tagged PDZ-RhoGEF (FL-PDZ-RhoGEF) was expressed together with Dvl2-EGFP and Celsr1-Myc in either MDCK or HA-DAAM1-expressing MDCK cells. Arrows point to cell-cell contacts where Dvl2-EGFP and Celsr1-Myc are both highly concentrated. Densitometric traces of FL-PDZ-RhoGEF fluorescence in control and HA-DAAM1-expressing MDCK cells are shown at the right. Positions for the tracing are shown in the inset. The peak marked with ''1'' corresponds to the signal at the junction marked with the same number. ''2'' is a junction showing little coaccumulation of Dvl2-EGFP and Celsr1-Myc. Densitometric analysis of FL-PDZ-RhoGEF fluorescence detected no significant differences between the ''1'' and ''2'' junctions in control cells, whereas in HA-DAAM1 cells, the fluorescence was 60% stronger at ''1'' than at ''2.'' Scale bars, 10 μm.

(E) FL-PDZ-RhoGEF was coexpressed with Dvl2-EGFP and Celsr1-Myc in HA-DAAM1-expressing MDCK cells. Endogenous ROCK1 was immunostained. Arrows point to cell-cell contacts where staining for ROCK1 increased together with other introduced proteins. Staining for Celsr1-Myc is not shown. Densitometric trace of the ROCK1 fluorescence is shown at the right. The peaks marked with ''1'' to ''3'' indicate the signal at the junctions marked with the same numbers. Scale bar, 10 μm.

In each panel of this figure, expression and localization of indicated proteins were visualized by fluorescence from EGFP or immunohistochemical staining with appropriate antibodies.

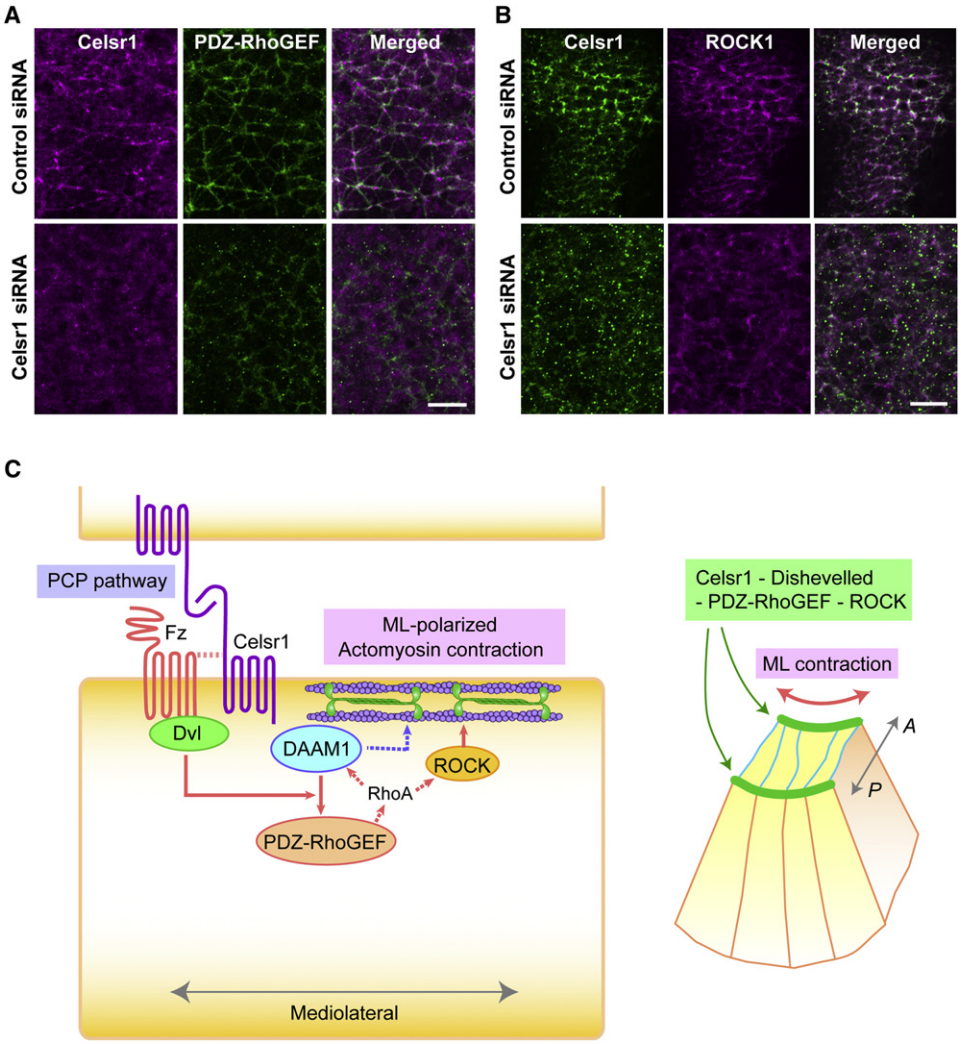

Figure 7. Celsr1 Establishes Polarized Distribution of PDZ-RhoGEF and ROCK1

(A and B) Effects of Celsr1 depletion on the distribution of PDZ-RhoGEF (A) or ROCK1 (B) at the apical surfaces of neural plates. Embryos were electroporated with Celsr1-specific or control siRNAs and fixed at stage 8. Flat-mount samples were costained for Celsr1 and PDZ-RhoGEF or ROCK1. Scale bars, 10 μm.

(C) Summary of the present observations. Fz, Frizzled; Dvl, Dishevelled; ML, mediolateral. Arrows indicate the activation or modulation of a molecule or promotion of molecular interactions. Dotted arrows, hypothetical pathways. RhoA activated by PDZ-RhoGEF might lead to not only ROCK activation but also DAAM1 activation forming a positive feedback loop. DAAM1 might independently regulate F-actin.

See also Figure S6.

This type of cellular behavior is reminiscent of that seen in *Drosophila* epithelium undergoing germband extension (Bertet et al., 2004; Blankenship et al., 2006), strongly suggesting that epithelial cells use a similar strategy for their rearrangement in both vertebrates and invertebrates. In the case of *Drosophila* germband extension, the anisotropic contraction of actomyosin is used solely for convergent extension of the tissue. In the neural plate, however, convergent extension accompanies the bending of epithelial sheets. Different tissues likely employ modified versions of this conserved strategy for their own patterning. To summarize, our results suggest that the PCP-mediated, polarized constriction of neuroepithelial AJs induces convergence of their apical domains toward the midline of the neural plate; the resultant shrinkage of the plate at the apical edges causes its inward bending.

EXPERIMENTAL PROCEDURES

Expression Plasmids, siRNAs, and Recombinant Proteins

An expression plasmid for human PDZ-RhoGEF was kindly provided by K. Nagata and subcloned into the p3xFLAG vector (SIGMA). An expression plasmid for Myc-tagged human Celsr1 was kindly provided by E. Fuchs. Complementary DNAs for mouse DAAM1, Dishevelled-2, and Frizzled-6 were obtained from the FANTOM 3 cDNA library and subcloned into either pCMV-Tag2 or pCA vectors. Constructs for Xdd1 were prepared as described previously (Sokol, 1996). Custom-synthesized siRNA oligos (Stealth RNAs) were purchased from Invitrogen. The target sequences for siRNAs and

additional information on RNAi experiments are described in the Extended Experimental Procedures. Bacterial expression plasmids for glutathione S-transferase (GST)-tagged proteins were constructed with pGEX-4T or pGEX-6P vectors (GE Healthcare). Recombinant proteins were expressed in an *E. coli* BL21 strain and purified by use of glutathione (GSH) Sepharose beads (GE Healthcare). In the case of DAAM1-C protein, the GST-tag was removed by PreScission protease (GE Healthcare) treatment of GSH Sepharose beads.

Immunological Procedures and RhoGEF Activity Measurement

The details for antibody preparation and other immunological methods are described in the Extended Experimental Procedures. RhoGEF activity was measured by using RhoGEF exchange assay Biochem Kit (Cytoskeleton).

Cell Transfection

Cells were transfected with expression plasmids or siRNAs using Lipofectamine 2000 (Invitrogen). Stable transfectants were selected and maintained in culture medium containing 400 μg/ml of Hygromycin B. The cells were immunostained as described in the Extended Experimental Procedures. Images were obtained with a laser-scanning confocal microscope LSM710 (Carl Zeiss) equipped with a Plan Apochromat 63×/1.4 lens (Carl Zeiss).

Manipulation of Chicken Embryos

For manipulation of chicken embryos, we used the modified New culture method, as described previously (Nakaya et al., 2008). Electroporation was performed using a TSS20 Ovodyne electroporator (Intracel) at the following setting: 6 V, 3 pulses for 50 ms with 200 ms intervals. Cryosections of embryos and whole-mount neural tubes were prepared and immunostained as described in the Extended Experimental Procedures. Microscopic images were obtained with a laser-scanning confocal microscope LSM710 (Carl Zeiss) equipped with αPlan-NEOFLUAR 20×/0.50 lens (Carl Zeiss) for tissue sections or αPlan-FLUAR 100×/1.45 lens (Carl Zeiss) for whole-mount specimens.

Time-Lapse Imaging

For time-lapse imaging of the neural tube, chicken embryo cultures expressing EGFP-labeled MLC were transferred onto 0.3% agarose/33% albumin/saline prepared on glass-bottom dishes (IWAKI) at stage 7, then covered with 0.25% agarose/PBS. Time-lapse imaging was performed using a spinning-disc laser confocal microscope IX71 (Olympus) equipped with CSU-X1 (Yokogawa) and a LUCPlanFLN 40×/0.60 lens. Pictures were taken every 5 min and processed using Metamorph software (Molecular Devices) and ImageJ software (NIH).

SUPPLEMENTAL INFORMATION

Supplemental Information includes Extended Experimental Procedures, six figures, and four movies and can be found with this article online at doi:10.1016/j.cell.2012.04.021.

ACKNOWLEDGMENTS

We thank Y. Nakaya for advice on chicken embryology; E. Fuchs for Celsr1 plasmids; K. Nagata for the PDZ-RhoGEF plasmid; A. Sugimoto for an EM-CCD camera; T. Nagai for computational modeling; and the RIKEN Integrated Cluster of Clusters for computation facilities. We are also grateful to T. Uemura for discussion and H. Saito, M. Nomura-Harata, H. Sylvain, Y. Inoue, S. Kobayashi, H. Abe-Ishigami, and C. Uemura-Yoshii for their technical support. This work was supported by grants from the programs Grants-in-Aid for Specially Promoted Research (to M.T.), for Scientific Research-C (to H.H.), and for Young Scientists-B (to T.N.) from the Japan Society for Promotion of Science.

Received: June 14, 2011
Revised: September 13, 2011
Accepted: April 5, 2012
Published: May 24, 2012

REFERENCES

Alvarez, I.S., and Schoenwolf, G.C. (1992). Expansion of surface epithelium provides the major extrinsic force for bending of the neural plate. J. Exp. Zool. *261*, 340–348.

Aspenström, P., Richnau, N., and Johansson, A.S. (2006). The diaphanous-related formin DAAM1 collaborates with the Rho GTPases RhoA and Cdc42, CIP4 and Src in regulating cell morphogenesis and actin dynamics. Exp. Cell Res. *312*, 2180–2194.

Bertet, C., Sulak, L., and Lecuit, T. (2004). Myosin-dependent junction remodelling controls planar cell intercalation and axis elongation. Nature *429*, 667–671.

Blankenship, J.T., Backovic, S.T., Sanny, J.S., Weitz, O., and Zallen, J.A. (2006). Multicellular rosette formation links planar cell polarity to tissue morphogenesis. Dev. Cell *11*, 459–470.

Chen, W.S., Antic, D., Matis, M., Logan, C.Y., Povelones, M., Anderson, G.A., Nusse, R., and Axelrod, J.D. (2008). Asymmetric homotypic interactions of the atypical cadherin flamingo mediate intercellular polarity signaling. Cell *133*, 1093–1105.

Copp, A.J., Greene, N.D., and Murdoch, J.N. (2003). The genetic basis of mammalian neurulation. Nat. Rev. Genet. *4*, 784–793.

Curtin, J.A., Quint, E., Tsipouri, V., Arkell, R.M., Cattanach, B., Copp, A.J., Henderson, D.J., Spurr, N., Stanier, P., Fisher, E.M., et al. (2003). Mutation of Celsr1 disrupts planar polarity of inner ear hair cells and causes severe neural tube defects in the mouse. Curr. Biol. *13*, 1129–1133.

Devenport, D., and Fuchs, E. (2008). Planar polarization in embryonic epidermis orchestrates global asymmetric morphogenesis of hair follicles. Nat. Cell Biol. *10*, 1257–1268.

Etheridge, S.L., Ray, S., Li, S., Hamblet, N.S., Lijam, N., Tsang, M., Greer, J., Kardos, N., Wang, J., Sussman, D.J., et al. (2008). Murine dishevelled 3 functions in redundant pathways with dishevelled 1 and 2 in normal cardiac outflow tract, cochlea, and neural tube development. PLoS Genet. *4*, e1000259.

Formstone, C.J., and Mason, I. (2005). Expression of the Celsr/flamingo homologue, c-fmi1, in the early avian embryo indicates a conserved role in neural tube closure and additional roles in asymmetry and somitogenesis. Dev. Dyn. *232*, 408–413.

Habas, R., Kato, Y., and He, X. (2001). Wnt/Frizzled activation of Rho regulates vertebrate gastrulation and requires a novel Formin homology protein Daam1. Cell *107*, 843–854.

Häcker, U., and Perrimon, N. (1998). DRhoGEF2 encodes a member of the Dbl family of oncogenes and controls cell shape changes during gastrulation in Drosophila. Genes Dev. *12*, 274–284.

Haigo, S.L., Hildebrand, J.D., Harland, R.M., and Wallingford, J.B. (2003). Shroom induces apical constriction and is required for hingepoint formation during neural tube closure. Curr. Biol. *13*, 2125–2137.

Hamblet, N.S., Lijam, N., Ruiz-Lozano, P., Wang, J., Yang, Y., Luo, Z., Mei, L., Chien, K.R., Sussman, D.J., and Wynshaw-Boris, A. (2002). Dishevelled 2 is essential for cardiac outflow tract development, somite segmentation and neural tube closure. Development *129*, 5827–5838.

Hildebrand, J.D. (2005). Shroom regulates epithelial cell shape via the apical positioning of an actomyosin network. J. Cell Sci. *118*, 5191–5203.

Hildebrand, J.D., and Soriano, P. (1999). Shroom, a PDZ domain-containing actin-binding protein, is required for neural tube morphogenesis in mice. Cell *99*, 485–497.

Honda, H., Nagai, T., and Tanemura, M. (2008). Two different mechanisms of planar cell intercalation leading to tissue elongation. Dev. Dyn. *237*, 1826–1836.

Hong, E., and Brewster, R. (2006). N-cadherin is required for the polarized cell behaviors that drive neurulation in the zebrafish. Development *133*, 3895–3905.

Jacobson, A.G., and Gordon, R. (1976). Changes in the shape of the developing vertebrate nervous system analyzed experimentally, mathematically and by computer simulation. J. Exp. Zool. *197*, 191–246.

Keller, R., Shih, J., and Sater, A. (1992). The cellular basis of the convergence and extension of the Xenopus neural plate. Dev. Dyn. *193*, 199–217.

Kinoshita, N., Sasai, N., Misaki, K., and Yonemura, S. (2008). Apical accumulation of Rho in the neural plate is important for neural plate cell shape change and neural tube formation. Mol. Biol. Cell *19*, 2289–2299.

Kitzing, T.M., Sahadevan, A.S., Brandt, D.T., Knieling, H., Hannemann, S., Fackler, O.T., Grosshans, J., and Grosse, R. (2007). Positive feedback between Dia1, LARG, and RhoA regulates cell morphology and invasion. Genes Dev. *21*, 1478–1483.

Kölsch, V., Seher, T., Fernandez-Ballester, G.J., Serrano, L., and Leptin, M. (2007). Control of Drosophila gastrulation by apical localization of adherens junctions and RhoGEF2. Science *315*, 384–386.

Li, D., Hallett, M.A., Zhu, W., Rubart, M., Liu, Y., Yang, Z., Chen, H., Haneline, L.S., Chan, R.J., Schwartz, R.J., et al. (2011). Dishevelled-associated activator of morphogenesis 1 (Daam1) is required for heart morphogenesis. Development *138*, 303–315.

Liu, W., Sato, A., Khadka, D., Bharti, R., Diaz, H., Runnels, L.W., and Habas, R. (2008). Mechanism of activation of the Formin protein Daam1. Proc. Natl. Acad. Sci. USA *105*, 210–215.

Lu, J., Meng, W., Poy, F., Maiti, S., Goode, B.L., and Eck, M.J. (2007). Structure of the FH2 domain of Daam1: implications for formin regulation of actin assembly. J. Mol. Biol. *369*, 1258–1269.

Martin, A.C., Gelbart, M., Fernandez-Gonzalez, R., Kaschube, M., and Wieschaus, E.F. (2010). Integration of contractile forces during tissue invagination. J. Cell Biol. *188*, 735–749.

McNeill, H. (2010). Planar cell polarity: keeping hairs straight is not so simple. Cold Spring Harb. Perspect. Biol. *2*, a003376.

Nagai, T., and Honda, H. (2001). A dynamic cell model for the formation of epithelial tissue. Philos. Mag. B *81*, 699–719.

Nakaya, Y., Sukowati, E.W., Wu, Y., and Sheng, G. (2008). RhoA and microtubule dynamics control cell-basement membrane interaction in EMT during gastrulation. Nat. Cell Biol. *10*, 765–775.

Nishimura, T., and Takeichi, M. (2008). Shroom3-mediated recruitment of Rho kinases to the apical cell junctions regulates epithelial and neuroepithelial planar remodeling. Development *135*, 1493–1502.

Ravni, A., Qu, Y., Goffinet, A.M., and Tissir, F. (2009). Planar cell polarity cadherin Celsr1 regulates skin hair patterning in the mouse. J. Invest. Dermatol. *129*, 2507–2509.

Schoenwolf, G.C. (1991). Cell movements driving neurulation in avian embryos. Development *2* (*Suppl 2*), 157–168.

Simons, M., and Mlodzik, M. (2008). Planar cell polarity signaling: from fly development to human disease. Annu. Rev. Genet. *42*, 517–540.

Sokol, S.Y. (1996). Analysis of Dishevelled signalling pathways during Xenopus development. Curr. Biol. *6*, 1456–1467.

Strutt, D.I., Weber, U., and Mlodzik, M. (1997). The role of RhoA in tissue polarity and Frizzled signalling. Nature *387*, 292–295.

Usui, T., Shima, Y., Shimada, Y., Hirano, S., Burgess, R.W., Schwarz, T.L., Takeichi, M., and Uemura, T. (1999). Flamingo, a seven-pass transmembrane cadherin, regulates planar cell polarity under the control of Frizzled. Cell *98*, 585–595.

Vladar, E.K., Antic, D., and Axelrod, J.D. (2009). Planar cell polarity signaling: the developing cell's compass. Cold Spring Harb. Perspect. Biol. *1*, a002964.

Wallingford, J.B. (2006). Planar cell polarity, ciliogenesis and neural tube defects. Hum. Mol. Genet. *15* (Spec No 2), R227–R234.

Wallingford, J.B., Rowning, B.A., Vogeli, K.M., Rothbächer, U., Fraser, S.E., and Harland, R.M. (2000). Dishevelled controls cell polarity during Xenopus gastrulation. Nature *405*, 81–85.

Wang, J., Hamblet, N.S., Mark, S., Dickinson, M.E., Brinkman, B.C., Segil, N., Fraser, S.E., Chen, P., Wallingford, J.B., and Wynshaw-Boris, A. (2006). Dishevelled genes mediate a conserved mammalian PCP pathway to regulate convergent extension during neurulation. Development *133*, 1767–1778.

Watanabe, T., Hosoya, H., and Yonemura, S. (2007). Regulation of myosin II dynamics by phosphorylation and dephosphorylation of its light chain in epithelial cells. Mol. Biol. Cell *18*, 605–616.

Wei, L., Roberts, W., Wang, L., Yamada, M., Zhang, S., Zhao, Z., Rivkees, S.A., Schwartz, R.J., and Imanaka-Yoshida, K. (2001). Rho kinases play an obligatory role in vertebrate embryonic organogenesis. Development *128*, 2953–2962.

Winter, C.G., Wang, B., Ballew, A., Royou, A., Karess, R., Axelrod, J.D., and Luo, L. (2001). Drosophila Rho-associated kinase (Drok) links Frizzled-mediated planar cell polarity signaling to the actin cytoskeleton. Cell *105*, 81–91.

Ybot-Gonzalez, P., Savery, D., Gerrelli, D., Signore, M., Mitchell, C.E., Faux, C.H., Greene, N.D., and Copp, A.J. (2007). Convergent extension, planar-cell-polarity signalling and initiation of mouse neural tube closure. Development *134*, 789–799.